MCM-41-supported platinum carbonyl cluster-derived catalysts for asymmetric and nonasymmetric hydrogenation reactions

Susmit Basu [b], Maitri Mapa [c], Chinnakonda S. Gopinath [c], Mukesh Doble [d], Sumit Bhaduri [a,*], Goutam Kumar Lahiri [b,*]

[a] *Reliance Industries Limited, Swastik Mills Compound, V.N. Purav Marg, Chembur, Mumbai 400071, India*
[b] *Department of Chemistry, Indian Institute of Technology – Bombay, Powai, Mumbai 400076, India*
[c] *Catalysis Division, National Chemical Laboratory, Pune 411008, India*
[d] *Department of Biotechnology, Indian Institute of Technology – Madras, Chennai 600036, India*

Abstract

Anionic platinum carbonyl cluster ($[Pt_{12}(CO)_{24}]^{2-}$) was ion-paired with the 3-chloropropyltrimethoxysilyl-ammonium group chemically bound to the surface of MCM-41. The materials undergo quick decarbonylation and have been characterized before decarbonylation by IR and UV–vis spectroscopy and after decarbonylation by XPS and TEM. They have been used as catalysts for the hydrogenations of methyl pyruvate, acetophenone, nitrobenzene, benzonitrile, and ethylacetoacetate. The support and the quaternary ammonium groups have significant effects on surface platinum concentration, crystallite size, and observed activity. In the hydrogenation of the prochiral substrates methyl pyruvate or acetophenone, the cinchonidine-based catalyst gives significant enantioselectivity under optimum conditions. A kinetic model that includes an enantioselective product-formation step and a hydrogen pressure-dependent step for the deactivation of the enantioselective sites gives reasonable agreement between predicted and observed enantioselectivity. The model is also in accordance with the XPS and TEM data.

Keywords: Platinum carbonyl cluster; Hydrogenation catalysts; Functionalized MCM-41; Enantioselectivity; Asymmetric/non-asymmetric catalysis

1. Introduction

Insoluble polymer-supported homogeneous catalysts are of interest because they provide a simple and easy method for catalyst separation [1–7]. Grafting of proven asymmetric homogeneous catalysts onto a solid support is a viable strategy; however, this approach involves multistep syntheses of expensive chiral ligands and/or functionalization of a given support with such ligands [6,8–12]. Another strategy that has been the focus of much research avoids the costly synthesis of expensive ligands and/or organometallic complexes. Here a conventional heterogeneous catalyst, such as platinum or raney nickel, is modified by treatment with readily available chiral substances [13–33]. Although the overall success of this approach has been limited, platinum on alumina modified by cinchona alkaloids has been found to be a particularly effective catalyst for the enantioselective hydrogenation of α-ketoesters in general and pyruvate esters in particular [21–33]. This reaction is commonly referred to as the Orito reaction, in honor of its discoverer.

The potential of Chini clusters as homogeneous and supported catalysts has been extensively investigated [32–56]. We reported hydrogenation of ketones where the Chini cluster $[Pt_{12}(CO)_{24}]^{2-}$ ion paired on functionalized fumed silica was used as the precatalyst [32]. The catalyst was found to be more active than the material obtained by physical adsorption of $[Pt_{12}(CO)_{24}]^{2-}$ on the support.

Recently, we also showed that an enantioselective catalyst could be obtained by this general method of catalyst synthesis [43]. In the present paper we present detailed characterization and other studies on MCM-41-supported catalysts. MCM-41 was functionalized with chiral and nonchiral quaternary am-

monium groups, and the cluster-derived materials were tested as hydrogenation catalysts for chiral and nonchiral substrates. A simple kinetic model that rationalizes the observed dependence of enantioselectivity on hydrogen pressure in methyl pyruvate and acetophenone hydrogenation and is also consistent with the XPS and TEM results is presented.

2. Experimental

All preparations and manipulations were performed using standard Schlenk techniques under nitrogen atmosphere. Solvents were dried by standard procedures (toluene over Na/benzophenone; methanol over Mg turnings/iodine), distilled under nitrogen, and used immediately. Chloroplatinic acid was purchased from Johnson Mathey. Methyl pyruvate, methyl lactate, cinchonidine, colloidal silica, and benzylamine were purchased from Fluka. (3-Chloropropyl)trimethoxysilane, 1-phenylethanol, triethylamine, 3-hydroxybutyrate, and acetophenone were obtained from Aldrich. Benzonitrile and ethylacetoacetate were purchased from Spectrochem Pvt. Ltd. Nitrobenzene and aniline were obtained from Merck Ltd. MCM-41 and $Na_2[Pt_{12}(CO)_{24}]$ were synthesized as described previously [57,58]. All of the hydrogenation reactions were carried out in an autoclave. Conversions and enantioselectivities of the hydrogenation reactions with different substrates were monitored by gas chromatography (GC) with flame ionization detection (Shimadzu GC-14A gas chromatograph) using a chiral capillary column (112-2562 CYCLODEXB, J&W Scientific; length, 60 m; i.d., 0.25 mm; film, 0.25 μm). All hydrogenated products were initially identified using authentic commercial samples of the expected products. For methyl pyruvate hydrogenation, the *R* isomer of methyl lactate was found to be the major product (i.e., enantiomer *A*). For 2-phenylethanol, the absolute configuration was not determined, but one enantiomer (i.e., *A*) was observed to be the major component on the basis of GC experiments. A Thermo Nicolet 320 FTIR spectrophotometer and a Jasco V-570 UV–vis spectrophotometer were used for recording IR and reflectance spectra, respectively. A Philips Panalytical X'Pert Pro diffractometer with Cu-K_{α_1} radiation source of wavelength 1.540598 Å was used for XRD analysis. Diffraction data were recorded between 1 and 25° 2θ at intervals of 0.01° 2θ. A scanning speed of 0.5° 2θ/min was used (automatic divergence slit system). An FEI Quanta 200 instrument (using tungsten filament as the electron beam source and a gaseous secondary electron detector) was used for ESEM and EDAX analysis. A JEOL 1200 EX transmission electron microscope was used for the surface analysis of catalysts. A VG Microtech Multilab ESCA 3000 spectrometer was used for the XPS studies.

2.1. Functionalization of MCM-41

MCM-41 (1 g) preheated under vacuum at 200 °C for 4 h was refluxed with 2 mL of (3-chloropropyl)trimethoxysilane and 20 mL of dry toluene at 110 °C for 160 h. The product was then separated by filtration and washed several times with dry toluene. The ^{29}Si NMR spectra (^{1}H coupling and decoupling) in each step match well with data reported previously [59].

2.2. Modification of functionalized MCM-41 by cinchonidine alkaloid

The chloropropylsilane-functionalized MCM-41 (1 g) and cinchonidine (0.25 g) were added in a 1:1 absolute ethanol–dry toluene mixture (40 mL). The mixture was heated to reflux at 110 °C for 96 h. It was then filtered and washed several times with dry toluene, followed by dry methanol.

2.3. Modification of functionalized MCM-41 by triethylamine

The chloropropylsilane-functionalized MCM-41 (1 g) and freshly distilled triethylamine (10 mL) were added in dry toluene (10 mL). The mixture was heated to reflux at 110 °C for 96 h. It was then filtered and washed thoroughly with dry toluene, followed by dry methanol.

2.4. Synthesis of catalysts ***1a*** and ***1b***

Dried cinchonidine-modified functionalized MCM-41 (1 g) was added in preformed green methanolic solution (15 mL) of $Na_2[Pt_{12}(CO)_{24}]$ (0.2 g) under carbon monoxide atmosphere. The mixture was stirred at 25 °C for 48 h. The solid material was filtered off and washed thoroughly with dry methanol, then dried under CO atmosphere (**1b**). Exactly the same procedure was used for the preparation of triethylamine-modified functionalized MCM-41 (**1a**).

2.5. Thermal activation of catalysts ***1a*** and ***1b***

The catalyst **1a** or **1b** (1 g) was taken in a three-necked round-bottomed flask (25 mL) equipped with nitrogen and vacuum adapters and flushed with nitrogen to remove any residual oxygen. The system was evacuated, then heated to 70 °C for 4 h under a continuous flow of hydrogen gas. During this process, the catalyst turned from green to gray. This gray material was used in catalytic experiments with suitable substrates.

2.6. Catalytic experiments with activated catalysts ***1a*** and ***1b***

In general, the catalytic runs were carried out at 27 °C in 2 mL of methanol contained in glass vials, with 25–70 mg of catalyst (**1a/b**) (∼0.75–2 mg platinum) and 0.5–2.0 mmol of substrate. The glass vial was placed in an autoclave, and hydrogen pressure in the range of 20–70 bar was applied. At the end of the catalytic run, the reaction mixture was subjected to GC, and the extent of conversion was calculated on the basis of the ratio of peak areas of starting material and the product.

2.7. Kinetic model for asymmetric hydrogenation

It is assumed that the rate of deactivation of the enantioselective sites is *n*th order with respect to H_2 pressure,

$$\frac{\mathrm{d}Pt}{\mathrm{d}t} = -k_1 H_2^n. \tag{1}$$

Integrating and assuming at $t = 0$, $Pt = Pt_0$,

$$Pt = -k_1 H_2^n t + Pt_0. \quad (2)$$

The rate of formation of the major enantiomer A is assumed to be first order with respect to Pt and mth order with respect to hydrogen pressure,

$$\frac{dA}{dt} = k_2 Pt H_2^m. \quad (3)$$

Substituting Eq. (2) in Eq. (3) and integrating Eq. (3) gives

$$A = k_2 Pt_0 H_2^m t - k_1 k_2 H_2^{n+m} t^2/2. \quad (4)$$

Data is collected at 1 h. Hence, substituting $t = 1$ and rearranging Eq. (4) gives

$$\frac{A}{H_2^m} = k_2 Pt_0 - \frac{k_1 k_2}{2} H_2^n. \quad (5)$$

Thus a plot of A/H_2^m against H_2^n should give a straight line.

3. Results and discussion

3.1. Synthesis and characterization of platinum carbonyls on the support

The functionalization of MCM-41 with trimethoxychloropropylsilane followed by further reactions with amines, including ephedrine, has been reported previously [60]. The latter material was used as a potential chiral catalyst in the alkylation of benzaldehyde by diethyl zinc and was found to give only moderate enantioselectivity. The method that we used for functionalization of MCM-41 is similar to the reported method with minor modifications (see Section 2). The structural formulations of the dominant and freshly prepared catalytic sites are shown in Scheme 1.

Table 1
Elemental analysis data

Catalysts	'Chloropropyl' group[a] (mmol/g)	Quaternary ammonium group[a] (mmol/g)	Platinum[b] (mmol/g)	Surface Pt/Si ratio[c]
1a	2.2	0.1	0.2	0.0021
1b	2.2	0.3	0.1	0.00053 (fresh) 0.002 (used)

[a] By elemental (C, H, N) analysis.
[b] Total platinum analyzed by ICP-AES technique.
[c] Surface Pt/Si by XPS.

Chemical analyses show that for **1a** and **1b**, the degree of functionalization with chloropropyl groups is similar, ~2 mmol/g (Table 1). However, differences in quaternary ammonium and platinum contents are observed. Degrees of incorporation of the quaternary ammonium groups seem to depend on the nature of the amine, with more amine incorporation observed with cinchonidine than with triethyl amine. A plausible explanation for this finding is that, due to different sizes, polarities, number of nitrogen atoms, and other factors, the two amines have different reactivities and modes of adsorption within the pores of MCM-41. This leads to a difference in the total content of nitrogen.

The observed nitrogen and chloropropyl values indicate that even after the treatment with excess amine, numerous chloropropyl groups remain unreacted. Consistent with the bulk chloropropyl content derived from microanalysis, a significant amount of chlorine on the surface is also detected by EDAX. Chemical and EDAX analyses for all of the samples did not re-

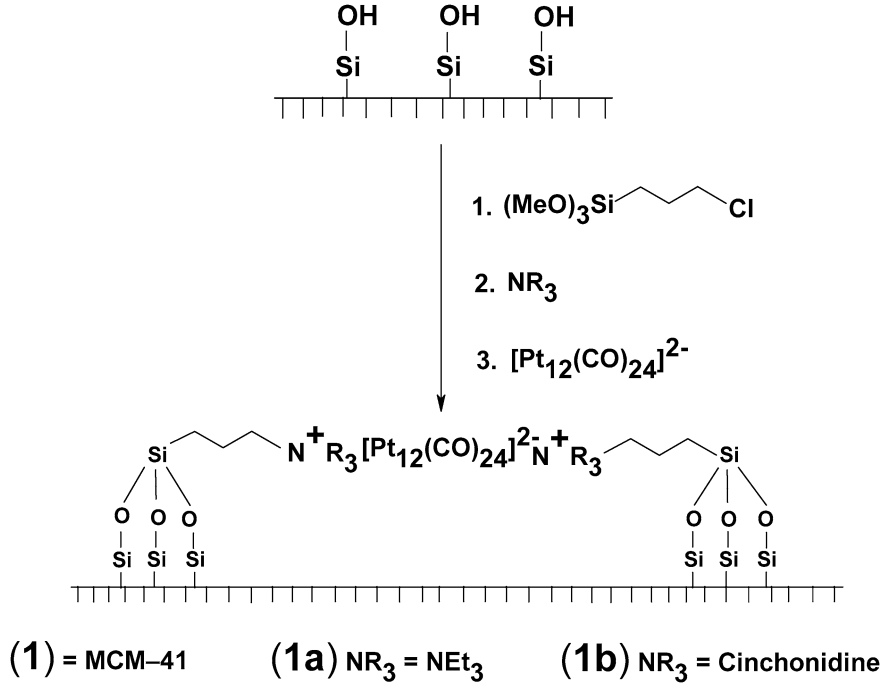

Scheme 1. Structural formulations of the freshly prepared catalysts.

veal the presence of sodium, ruling out physical adsorption of $Na_2[Pt_{12}(CO)_{24}]$ [32].

Both of the catalyst samples shown in Scheme 1, when freshly prepared, exhibit IR (at 2060 and 1850 cm^{-1}) and UV–vis (reflectance, 620 nm) bands that match well with the band of $[Pt_{12}(CO)_{24}]^{2-}$ [34]. However, as is evident from the disappearance of the characteristic IR and UV–vis bands, the CO ligands are lost quickly (<10 min) even when the samples are stored under CO. Therefore, the formulations shown in the scheme are applicable only to the materials before CO loss and the use of these materials as catalysts. Also, it must be emphasized once again that these formulations correspond only to the dominant and freshly prepared catalytic sites. It is very likely that there is more than one type of site, and some of these are IR and UV–vis silent. Note that, depending on the nature of the support, the decarbonylated Chini cluster may retain the cluster framework or undergo aggregation. The former behavior has been observed in zeolite Y; the latter, on MgO [44,45,50].

The powder XRD patterns of the catalysts and the functionalized MCM-41 derivatives closely match that of the reported pattern of MCM-41 [61]. Surface areas (m^2/g) and pore size distributions as measured by BET are as follows: for MCM-41, specific surface area, 740 and maximum cumulative area, 670; for **1a** and **1b**, specific surface area, 450 and maximum cumulative area, 410. These findings demonstrate that for each sample, internal surface area arising mainly from the mesopores is ~90% of the total surface area. In all of the MCM-41 derivatives, 90% the total pore volume comes from pores with radii of 1–2 nm, and ~1% of total pore volume is due to pores with radii of 1.9–2.0 nm. In addition, for both catalysts, the internal surface area makes up >90% of the total surface area. The decreased surface area on funtionalization observed here is consistent with earlier reports [62].

3.2. *Hydrogenation with catalysts **1a** and **1b***

Control experiments established that in solution, $[Bu_4N][Pt_{12}(CO)_{24}]$ as a homogeneous catalyst has negligible activity for the hydrogenation of methyl pyruvate, acetophenone, ethylacetoacetate, benzonitrile, and nitrobenzene. Prolonged contact of $[Bu_4N]_2[Pt_{12}(CO)_{24}]$ with cinchonidine or triethylamine leads to decomposition of the cluster and formation of colloidal platinum. The catalytic performance of **1a** was tested for all five substrates; the turnover numbers are given in Table 2. With nitrobenzene and methyl puruvate as the substrates, good turnovers are obtained for catalyst **1a**. Interestingly, that for all of the substrates except benzonitrile, the activity of **1a** is greater than the reported activity of an analogous fumed silica-based catalyst [32,34].

The enantioselectivity of catalyst **1b** was tested with two prochiral substrates: methyl pyruvate and acetophenone. With ethylacetoacetate (also a prochiral substrate), no enantioselectivity could be obtained. This may be due to differences in the mode of adsorption between ethylacetoacetate and methyl pyruvate and acetophenone. The enantioselectivities of **1b** in the hydrogenation of methyl pyruvate and acetophenone were evaluated under a wide variety of conditions (Table 3). As we reported earlier [43], with an analogous catalyst with fumed silica as the support, no enantioselectivity could be obtained under any of these conditions. In contrast, with **1b** as the catalyst for both of the substrates, varying enantioselectivities could be obtained (e.g., entries 4, 10, and 17 in Table 3 for both substrates and entries 11 and 19 for methyl pyruvate and for acetophenone, respectively). Thus, under optimum conditions, for methyl pyruvate and acetophenone, the best ee's obtained are ~95 and ~49%, respectively (entries 11 and 10, Table 3).

Unlike the classical Orito reaction, in which maximum enantioselectivity and rate are achieved only after a certain induction time [21,22], no such induction time is observed with **1b** as the catalyst. In our earlier report, the reaction was found to be approximately first order with respect to the concentrations

Table 2
Estimated TON (TOF in /min) for the hydrogenation processes[a]

Catalysts	Substrates				
	Nitro-benzene	Benzo-nitrile	Ethylaceto-acetate	Methyl pyruvate	Aceto-phenone
1a	700.0 (1.0)[b]	33.3 (0.5)	87.8 (1.5)	71.4 (1.2) 800.0 (1.1)[b]	45.5 (0.7)
1b	–	–	–	47.8 (0.8)	48.9 (0.8)

[a] Reaction conditions: 50 bar H_2 gas pressure, 1 mmol substrate, 70 mg catalyst, 1 h reaction time, temperature = 300 K, methanol solvent (2 mL). **1b** was tested only for the last two prochiral substrates. (TON = mmol of product formed per mmol of platinum, TOF = TON/60 unless specified otherwise.)
[b] Substrate: 10 mmol, time: 12 h (rest of the conditions are same) (TOF = TON/720).

Table 3
%conversion and %ee under varying substrate concentration and hydrogen pressure[a]

Entry No.	Amount substrate (mg)	Pressure (bar)	Methyl pyruvate		Acetophenone	
			Conversion (%)	%ee	Conversion (%)	%ee
1	60	20	50	~0	11	5
2		30	57	~0	20	10
3		40	53	~0	–	–
4		50	55	54	31	32
5		60	59	~0	23	20
6		70	–	–	28	4
7	120	20	45	3	12	2
8		30	50	~0	21	6
9		40	46	2	35	32
10		50	43	50	40	49
11		50[b]	15	95	–	–
12		60	–	–	28	21
13		70	46	5	29	15
14	240	20	35	5	12	3
15		30	47	2	21	6
16		40	42	4	21	26
17		50	44	16	28	23
18		60	–	–	34	21
19		70	33	~0	29	18

[a] Reaction conditions: methanol solvent (2 mL), 1 h reaction time, temperature = 300 K, with 70 mg **1b**. Each experiment was carried out in duplicate and the average values are given. The "–" refers to experiments where the difference in conversion between the two duplicate experiments was more than 5%.
[b] This data is of 15 min reaction time.

of the catalyst and methyl pyruvate [43]. The linear dependence of rate on substrate concentration is maintained over a range of hydrogen pressures. To a first approximation, the rate is pressure-invariant for methyl pyruvate and exhibits complex pressure dependence for acetophenone. As can be seen from Table 3, the most apparent and striking effect of hydrogen pressure is on enantioselectivity. The best enantioselectivity in methyl pyruvate hydrogenation is obtained at a pressure of 50 bar; all other pressures give negligible enantioselectivities. Similar observations are also made for acetophenone hydrogenation, but in this case the dependence of enantioselectivity on hydrogen pressure is less marked. A plausible explanation for this finding is provided in Section 3.3.

Both **1a** and **1b** were recycled three times without any noticeable drop in percent conversion. The enantioselectivity loss of **1b** with increased conversion is irreversible, and negligible enantioselectivities are observed for the second and the third run.

3.3. Kinetic model

As already mentioned, the enantioselectivity of both methyl pyruvate and acetophenone hydrogenations with **1b** as the catalyst shows a critical dependence on hydrogen pressure. A simple kinetic model that explains the essential features of the observed dependence of enantioselectivity on hydrogen pressure is discussed below. Further details were provided in Section 2.

The basic assumption behind the model is that there are enantioselective sites, but these sites are deactivated as the reactions progress, and the rate of deactivation is nth order with respect to H_2 pressure. It is also assumed that the rate of formation of the major enantiomer, A, is first order with respect to platinum and mth order with respect to hydrogen pressure. From these two differential equations, straightforward mathematical manipulations show that the plot of A/H_2^m against H_2^n should yield a straight line (see Section 2). Note that the inclusion of another step (i.e., the formation of racemic products at nonenantioselective sites) will increase the number of assumed rate constants to three without significantly improving the model. For this reason, we have not considered such a model.

Several different m and n were considered, and the values of m and n that gave the best model predictions were determined. Figs. 1 and 2 show these charts for methyl pyruvate ($n = 0.5$, $m = 1$) and acetophenone ($n = 0.5$, $m = 3$), respectively. In both cases, the R^2s for the linear regression lines are estimated to be $\geqslant 0.9$, indicating that the model predictions are good. Therefore, the modeling studies indicate that deactivation of the enantioselective sites for both methyl pyruvate and acetophenone are half-order reactions with respect to hydrogen pressure.

Nonetheless, the order of the major enantiomer formation reaction with respect to the hydrogen pressure is different for the two substrates. The best fits are obtained if the formations of the major enantiomers of methyl lactate and 1-phenylethanol are assumed to be first and third order, respectively, with respect to the hydrogen pressure. The half-order dependence of the deactivation of enantioselective sites on hydrogen pressure implies that deactivation is preceded by the dissociation of dihydrogen into dihydrides. The first-order dependence of enantioselective formation of methyl lactate on hydrogen pressure may be rationalized by stoichiometry; that is, two hydrogen atoms are added to the substrate to give the product. The third-order dependence of the enantioselective formation of 1-phenylethanol on hydrogen pressure is more difficult to rationalize. It probably indicates the formation of active sites with six hydride ligands before the product formation step where two hydrides are transferred to the substrates.

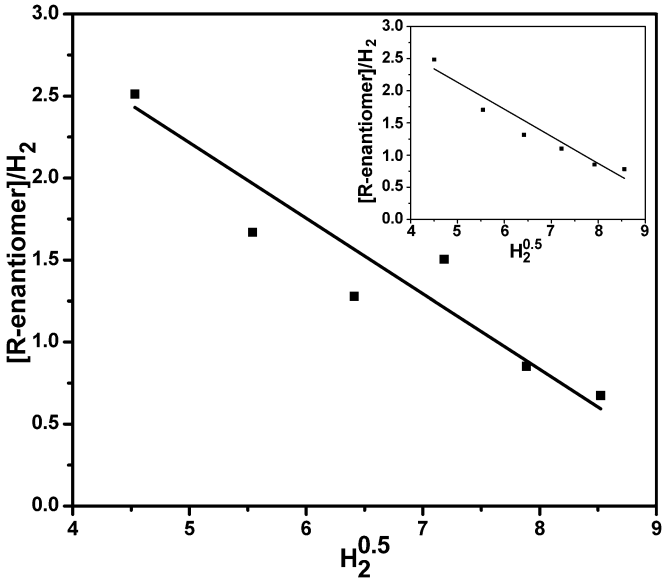

Fig. 1. Model prediction (least square fitted straight line) versus experimental data for methyl pyruvate (60 mg) hydrogenation. Inset shows the plot for 240 mg substrate. R-enantiomer is the major enantiomer and (■) are experimentally determined [R-enantiomer] values at different pressures.

3.4. XPS and TEM studies

Catalysts **1a** and **1b** were studied by XPS; the results are shown in Fig. 3. The spectra obtained for **1a** and **1b** are very similar, except the signal intensity of the former is nearly an order of magnitude more than that of **1b**. The bulk concentration of platinum in **1a** is only twice that of **1b**; that is, the surface platinum concentration in **1a** is much greater than what would be expected on the basis of bulk analysis. Therefore, the XPS data demonstrate that the nature of the quaternary ammonium group has a major effect on the surface concentration of platinum.

The broadening and small valley between the spin–orbit components for **1a** and **1b** indicate that two different Pt species are present. Deconvolution of the signal for **1b** shows species at 71 and 72.7 ± 0.1 eV with an intensity ratio of 5:1 [43]. This ratio is 10:1 for **1a**. The high-intensity Pt $4f$ component on both catalysts has a binding energy (BE) close to that of the reported value [63] for the free platinum clusters ($4f_{7/2} \sim 71.0$ eV). The high BE component is due to a Pt^{2+} species, probably $PtCl_2$ with coordinated organic moieties. Facile decarbonylation of the supported cluster is expected to cause a slight shift

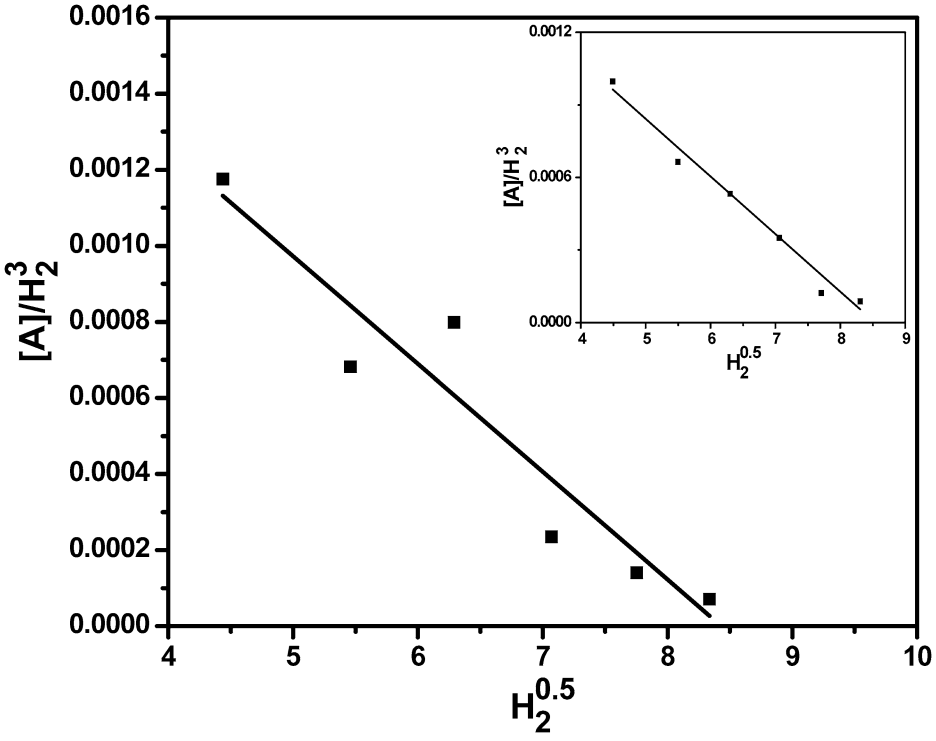

Fig. 2. Model prediction (least square fitted straight line) versus experimental data for acetophenone (60 mg) hydrogenation. Inset shows the plot for 120 mg substrate. *A*-enantiomer is the major enantiomer and (■) are experimentally determined [*A*-enantiomer] values at different pressures.

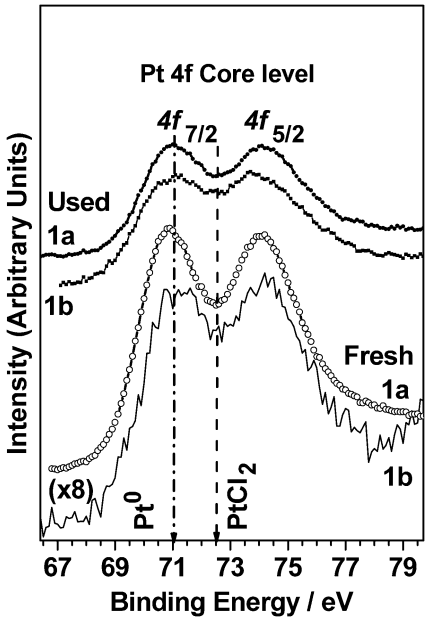

Fig. 3. Core level (platinum 4*f*) XPS spectra of fresh and used **1a**, **1b** (see text).

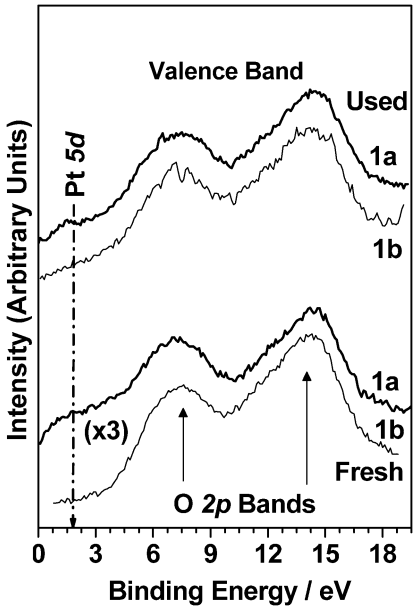

Fig. 4. Valence band (oxygen 2*p*, platinum 5*d*) XPS spectra of fresh and used **1a** and **1b** (see text).

toward lower platinum BE. Reaction between some of the decarbonylated clusters and excess tetralkyl ammonium chloride functionalities on the support probably leads to the formation of $PtCl_2$.

Fig. 4 shows the valence band spectra of the catalysts. Two oxygen 2*p*-derived bands, typical of MCM-41, and a Pt 5*d* band around 2 eV are observed for all of the catalysts. It may be noted that MCM-41 is a poor conductor and does not show any feature at the Fermi level. A notable increase in the density of states at the Fermi level (BE = 0 eV) on catalyst **1a** is probably due to relatively large platinum crystallites, which interact very weakly with MCM-41.

The electron counts and the Pt/Si ratio (Table 1) of the used catalyst **1b** are noticeably higher than those of fresh **1b**. The fact that the Pt/Si ratio is higher in the used catalyst than in the fresh catalyst may be attributed to the higher dispersion of the metallic particles in the used catalyst; however, it could also

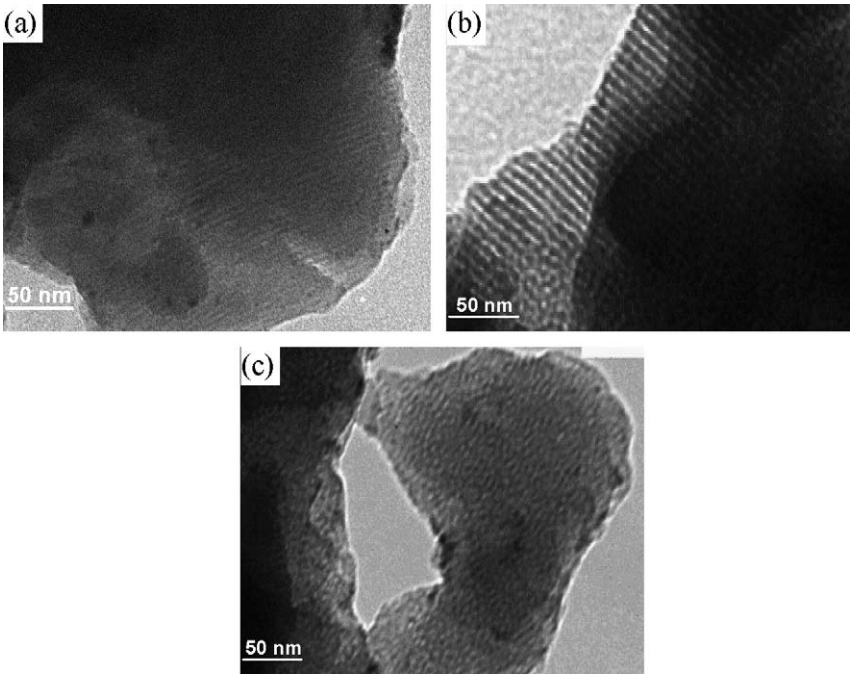

Fig. 5. TEM images of (a) fresh **1a**, (b) fresh **1b**, and (c) used **1b**.

indicate that in **1b**, before its use as a catalyst, the platinum sites are well dispersed within the pores and thus less accessible to ESCA. Agglomeration of such sites and migration of platinum crystallites out of the pores occur during catalysis. The TEM data (see below) support the latter conclusion. The Pt/Si ratios in the fresh catalysts are in the order of **1a** > **1b**.

TEM images of fresh **1a** and **1b** and used **1b** are shown in Figs. 5a–5c. The characteristic fringes typical of MCM-41 are visible in all of the micrographs. Relatively large (5–15 nm) platinum crystallites are seen in **1a** (Fig. 5a). The platinum crystallites seem to gather at the edges of the MCM-41 support. In contrast, in fresh **1b**, the platinum crystallites are well dispersed and located in the pores of MCM-41 (Fig. 5b). These crystallites must be smaller (<3 nm) than the fringe width (3.5 nm), and therefore they are not observed except for some line broadening at certain fringe spots (Fig. 5b). Thus, as indicated by XPS and confirmed by the TEM data, the amines used to functionalize MCM-41 have a profound effect on the size and distribution of the platinum sites. With cinchonidine as the amine, small platinum crystallites uniformly distributed within the mesopores of **1b** are obtained. After use in catalytic runs, changes are observed in the TEM images of **1b**. Some of the platinum crystallites agglomerate, and crystallite size increases (>6 nm). The agglomerated crystallites gather at the grain boundaries of MCM-41 (Fig. 5c). A plausible explanation for this finding that is consistent with the kinetic model and all of the physical characterization data is as follows. Most of the platinum crystallites in fresh **1b** are enantioselective, due to their smallness and their close proximity to the cinchonidium groups. From a crystallographic standpoint, the number of defect sites likely to be chiral on their own will be significantly greater for small (<3 nm) crystallites [64,65]. Combinations of some of these defect sites with chiral cinchonidium groups create diastereomeric sites that are responsible for the observed enantioselectivity. It is possible that the platinum crystallites in the fresh catalyst are achiral, and the chirality comes only from the cinchonidium group. Either way, the interaction of the substrate with these sites leads to diastereomers, which are expected to have different rate constants. The platinum crystallites are mobile under the conditions used for hydrogenation, and as the reaction proceeds, agglomeration of the platinum crystallites occurs, and thus the enantioselective, diastereomeric sites are deactivated. However, because the platinum crystallites are located within the narrow confines of the mesopores, mobility is restricted there, and deactivation takes long enough for significant enantioselectivity to be observed at relatively low conversions. Finally, it must be pointed out that in the absence of histograms of the particle size distribution versus diameter, the discussion on the size and distribution of the platinum sites is only speculative.

4. Conclusion

In conclusion, by ion-pairing $[Pt_{12}(CO)_{24}]^{2-}$ with chiral and nonchiral NR_4^+ groups chemically linked to the surface of MCM-41, we obtained catalysts for the hydrogenations of methyl pyruvate, acetophenone, nitrobenzene, benzonitrile, and ethylacetoacetate. The NR_4^+ group has a major effect on surface platinum concentration, crystallite size, and catalytic performance. In the hydrogenation of methyl pyruvate or acetophenone, significant enantioselectivities are obtained with the catalyst where NR_4^+ = cinchonidium. The critical dependence of enantioselectivity on hydrogen pressure can be explained by a simple kinetic model. We have offered a tentative explanation for the observed enantioselectivity that takes into account the kinetic model, XPS, and TEM data.

Acknowledgments

Financial assistance from Reliance Industries Ltd., Mumbai, India and the University Grant Commission, New Delhi, India is gratefully acknowledged.

References

[1] M. Lemaire, Pure Appl. Chem. 76 (2004) 679.
[2] P. McMorn, G.J. Hutchings, Chem. Soc. Rev. 33 (2004) 108.
[3] D.E. Bergbreiter, Chem. Rev. 102 (2002) 3345.
[4] J.A. Gladysz, Chem. Rev. 102 (2002) 3215.
[5] C.A. McNamara, M.J. Dixon, M. Bradely, Chem. Rev. 102 (2002) 3275.
[6] C.E. Song, S. Lee, Chem. Rev. 102 (2002) 3495.
[7] N.E. Leadbeater, M. Marco, Chem. Rev. 102 (2002) 3217.
[8] P.N. Liu, P.M. Gu, F. Wang, Y.Q. Tu, Org. Lett. 6 (2004) 169.
[9] A. Hu, H.L. Ngo, W. Lin, J. Am. Chem. Soc. 125 (2003) 11490.
[10] J.M. Thomas, B.F.G. Johnson, R. Raja, G. Sankar, P.A. Midgley, Acc. Chem. Res. 36 (2003) 20.
[11] B.F.G. Johnson, S.A. Raynor, D.S. Shephard, T. Mashmeyer, J.M. Thomas, G. Sankar, S. Bromley, R. Oldroyd, L. Gladden, M.D. Mantle, Chem. Commun. (1999) 1167.
[12] Q.-H. Fan, Y.-M. Li, A.S.C. Chan, Chem. Rev. 102 (2002) 3385.
[13] N. Bonalumi, A. Vargas, D. Ferri, T. Bürgi, T. Mallat, A. Baiker, J. Am. Chem. Soc. 127 (2005) 8467.
[14] T. Bürgi, A. Baiker, Acc. Chem. Res. 37 (2004) 909.
[15] K. Balázsik, M. Bartók, J. Catal. 224 (2004) 463.
[16] R. Strobel, F. Krumeich, W.J. Stark, S.E. Pratsinis, A. Baiker, J. Catal. 222 (2004) 307.
[17] M.S. Schneider, A. Urakawa, J.-D. Grunwaldt, T. Bürgi, A. Baiker, Chem. Commun. (2004) 744.
[18] S.C. Mhadgut, I. Bucsi, M. Török, B. Török, Chem. Commun. (2004) 984.
[19] N. Haruna, D.E. Acosta, S. Nakagawa, K. Yamaguchi, A. Tai, T. Okuyama, T. Sugimura, Heterocycles 62 (2004) 375.
[20] C. Exner, A. Pfaltz, M. Studer, H.-U. Blaser, Adv. Synth. Catal. 345 (2003) 1253.
[21] M. Bartók, M. Sutyinszki, K. Felföldi, J. Catal. 220 (2003) 207.
[22] X. Li, R.P.K. Wells, P.B. Wells, G.J. Hutchings, Catal. Lett. 89 (2003) 163.
[23] M. Studer, H.-U. Blaser, C. Exner, Adv. Synth. Catal. 345 (2003) 45, and references therein.
[24] H.-U. Blaser, H.-P. Jalett, M. Müller, M. Studer, Catal. Today 37 (1997) 441.
[25] A. Baiker, J. Mol. Catal. A: Chem. 163 (2000) 205.
[26] M. Studer, S. Burkhardt, H.-U. Blaser, Chem. Commun. (1999) 1727.
[27] C. LeBlond, J. Wang, J. Liu, A.T. Andrews, Y.-K. Sun, J. Am. Chem. Soc. 121 (1999) 4920.
[28] K. Balázsik, K. Szöri, K. Felföldi, B. Török, M. Bartók, Chem. Commun. (2000) 555.
[29] M. Studer, S. Burkhardt, A.F. Indolese, H.-U. Blaser, Chem. Commun. (2000) 1327.
[30] M. von Arx, T. Mallat, A. Baiker, Angew. Chem. Int. Ed. 40 (2001) 2302.
[31] M. Sutyinszki, K. Szöri, K. Felföldi, M. Bartók, Catal. Commun. 3 (2002) 125.
[32] H. Paul, S. Basu, S. Bhaduri, G.K. Lahiri, J. Organomet. Chem. 689 (2004) 309.
[33] H. Paul, S. Bhaduri, G.K. Lahiri, Indian J. Chem. A 42 (2003) 2392.
[34] H. Paul, S. Bhaduri, G.K. Lahiri, Organometallics 22 (2003) 3019.
[35] S. Bhaduri, G.K. Lahiri, D. Mukesh, H. Paul, K. Sarma, Organometallics 20 (2001) 3329.
[36] S. Bhaduri, Curr. Sci. 78 (2000) 1318, and references therein.
[37] S. Bhaduri, G.K. Lahiri, P. Munshi, D. Mukesh, Catal. Lett. 65 (2000) 61.
[38] S. Bhaduri, P. Mathur, P. Payra, K. Sharma, J. Am. Chem. Soc. 120 (1998) 12127.
[39] S. Bhaduri, K. Sharma, J. Chem. Soc., Chem. Commun. (1996) 207.
[40] S. Bhaduri, V.S. Darshane, K. Sharma, D. Mukesh, J. Chem. Soc., Chem. Commun. (1992) 1738.
[41] S. Bhaduri, K.R. Sharma, J. Chem. Soc., Dalton Trans. (1984) 2309.
[42] S. Bhaduri, K.R. Sharma, J. Chem. Soc., Dalton Trans. (1982) 727.
[43] S. Basu, H. Paul, C.S. Gopinath, S. Bhaduri, G.K. Lahiri, J. Catal. 229 (2005) 298.
[44] A. Fukuoka, N. Higashimoto, Y. Sakamoto, S. Inagaki, Y. Fukushima, M. Ichikawa, Microporous Mesoporous Mater. 48 (2001) 171.
[45] J.G.-C. Shen, J. Phys. Chem. B 104 (2000) 423.
[46] G. Sastre, N. Raj, C.R.A. Catlow, R. Roque-Malherbe, A. Corma, J. Phys. Chem. B 102 (1998) 3198.
[47] A. Fukuoka, M. Osada, T. Shido, S. Inagaki, Y. Fukushima, M. Ichikawa, Inorg. Chim. Acta 294 (1999) 281.
[48] M. Sasaki, M. Osada, N. Sugimoto, S. Inagaki, Y. Fukushima, A. Fukuoka, M. Ichikawa, Microporous Mesoporous Mater. 21 (1998) 597.
[49] T. Yamamoto, T. Shido, S. Inagaki, Y. Fukushima, M. Ichikawa, J. Phys. Chem. B 102 (1998) 3866.
[50] M. Ichikawa, Adv. Catal. 38 (1992) 283.
[51] J.-R. Chang, D.C. Koningsberger, B.C. Gates, J. Am. Chem. Soc. 114 (1992) 6460.
[52] G.-J. Li, T. Fujimoto, A. Fukuoka, M. Ichikawa, Catal. Lett. 12 (1992) 171.
[53] G.-J. Li, T. Fujimoto, A. Fukuoka, M. Ichikawa, J. Chem. Soc., Chem. Commun. (1991) 1337.
[54] M. Ichikawa, J. Chem. Soc., Chem. Commun. (1976) 11.
[55] R. Raja, J.M. Thomas, M.D. Jones, B.F.G. Johnson, D.E.W. Vaughan, J. Am. Chem. Soc. 125 (2003) 14982, and references therein.
[56] M.D. Jones, R. Raja, J.M. Thomas, B.F.G. Johnson, D.W. Lewis, J. Rouzaud, K.D.M. Harris, Angew. Chem. Int. Ed. 42 (2003) 4326.
[57] J.S. Beck, J.C. Vartuli, W.J. Roth, M.E. Leonowicz, C.T. Kresge, K.D. Schmitt, C.T.-W. Chu, D.H. Olson, E.W. Sheppard, S.B. McCullen, J.B. Higgins, J.L. Schlenker, J. Am. Chem. Soc. 114 (1992) 10834.
[58] G. Longoni, P. Chini, J. Am. Chem. Soc. 98 (1976) 7225.
[59] E.J.R. Sudhölter, R. Huis, G.R. Hays, N.C.M. Alma, J. Colloid Interface Sci. 103 (1985) 554.
[60] T.M. Jyothi, M.L. Kaliya, M. Herskowitz, M.V. Landau, Chem. Commun. (2001) 992.
[61] R. Mokaya, Chem. Commun. (2001) 1092.
[62] S.-J. Huang, C.-H. Huang, W.-H. Chen, X. Sun, X. Zeng, H.-K. Lee, J.A. Ripmeester, C.-Y. Mou, S.-B. Liu, J. Phys. Chem. B 109 (2005) 681.
[63] G. Apai, S.-T. Lee, M.G. Mason, L.J. Gerenser, S.A. Gardner, J. Am. Chem. Soc. 101 (1979) 6880.
[64] D.S. Sholl, A. Asthagiri, T.D. Power, J. Phys. Chem. B 105 (2001) 4771.
[65] R. Narayanan, M.A. El-Sayed, J. Phys. Chem. B 109 (2005) 12663.